Classical approach to H_2^+-H(1*s*) collisions

D. Hennecart[1] and J. Pascale[2,*]

[1]*Centre Interdisciplinaire de Recherche Ions Lasers, CEA-CNRS-ISMRA–Université de Caen, 6 Boulevard Maréchal Juin, F-14050 Caen Cedex 04, France*

[2]*Service des Photons, Atomes et Molécules, CEA, CE Saclay, Bâtiment 522, F-91191 Gif sur Yvette Cedex, France*

(Received 20 July 2004; published 19 January 2005)

Collisions between H_2^+ ion projectiles with H targets have been investigated in the 2.5–1000 keV energy range by means of classical-trajectory Monte Carlo calculations. It has been possible to simulate classically a dynamical H_2^+ molecule and, therefore, the approach includes all the Coulomb interactions between the five classical particles. Particular attention is paid to the description of the H_2^+ ion projectile, initially in its first vibration (v=0) ground state, and to the identification of the various reaction products after collision. Total cross sections for all the possible reaction channels are calculated, and are found in fair agreement with recent experimental data in the 20–100 keV energy range. Final *n*-state distributions for the hydrogen fragments are also determined.

DOI: 10.1103/PhysRevA.71.012710 PACS number(s): 34.70.+e, 82.30.Fi, 52.20.Hv

I. INTRODUCTION

The well-known classical-trajectory Monte Carlo method (CTMC) [1] has been largely employed in the past to describe electron-capture and ionization processes occurring in collisions between ionic projectiles and atomic targets. But the use of this method was generally limited to one-electron atomic targets since multielectron atoms or molecules are classically unstable with respect to dissociation or autoionization. To avoid this problem, previous CTMC collision studies involving H_2^+ or H_2 molecular targets have developed one- or two-electron models, where the distance of the two protons is fixed at the equilibrium distance of the molecule and the assumption of independent electrons is made [2–4]. However, as the problem of nonstability of the molecule is attributed to the Heisenberg principle that is not taken into account in a classical description of the molecule, some efforts have been devoted in the past to simulate this principle in a classical theory.

Kirschbaum and Wilets [5] proposed a classical atomic model which incorporates features of the Heisenberg principle through analytical potentials. Doing this, they found that ground-state configuration energies of the He, Li, Ne, and Ar atoms are overestimated within 15% of their experimental or Hartree-Fock values, and the H_2^+ and H_2 molecules are considerably overbound. Cohen [6] observed that this overbinding is due to the localization of the electron(s) at high-symmetry positions, namely, at the molecular midpoint of H_2^+ or in the bisecting plane of H_2. In order to prevent this electron collapse, energy-dependent repulsive potentials were used in his model, leading to accurate ground-state configuration energies for H_2^+ and H_2. However, the determination of the parameters of the potentials is critical since they have to reproduce both the ground-state energy of the electron-parent ion system and the ground-state energy of the molecule without changing its stability. We found that this model leads to unrealistic electronic clouds for the H_2^+ and H_2 molecules, localized mainly in a plane. When used in collisions studies, the model is found very computing-time-consuming since many energy-dependent potentials must be evaluated at each step of the integration of the Hamilton equations. Moreover, since an electron has to stabilize around a nucleus, the use of the model in collision studies may lead to instability in the integration of the Hamilton equations.

More recently, Wood and Olson [7] and Olson and Feeler [8] have proposed a dynamical model of the H_2 molecule in collisions with an ion, in which each electron is initially bound by the Coulomb force to its parent ion and has no interaction either with the other ion of the molecule or with the other electron. The two atoms of the molecule are then bound by a Morse potential. During the collision, either the Coulomb electron-electron interaction is included in the Hamiltonian along with the Coulomb interactions between the electrons and the other ions or the Morse potential is slowly switched off, following the reaction channel considered in the collision.

Another approach, in the beginning of the present work, was proposed by Greenspan [9], who showed that it is possible to simulate classically a dynamical H_2^+ or H_2 molecule in its first vibration (v=0) ground state by considering all the Coulomb interactions between electron(s) and protons. Thus, given the experimental energy of the molecule in its ground state, the Hamilton equations for the multibody system are solved to determine the vibration motion of the protons correlated with the motion of the electron(s). Our classical method for simulating the H_2^+ molecular ion is basically the one described in full detail by Greenspan [9]. In the case of the H_2 molecule, Greenspan [9] also showed that under the assumption of an attractive Coulomb interaction between the electrons, the average experimental data for the vibration frequency and the equilibrium distance of H_2 could be well reproduced. We have not retained this unrealistic assumption when considering the H_2 molecule and have been able to reproduce as well the H_2 molecule by using the pure repul-

*Electronic address: j.pascale@free.fr

sive Coulomb interaction between the electrons.

In the present paper, we apply the CTMC method developed by Abrines and Percival [1] to the treatment of collisions, in the 2.5–1000 keV energy range, between H_2^+ projectiles and H(1*s*) targets. The 20–100 keV energy range is more particularly investigated as some recent experimental data are available in this range for various reaction channels [10]. In the course of the collision, all the mutual interactions between the particles are taken into account by using pure Coulomb potentials. This work shows that a stable molecular ion can be obtained if the initial position and momentum coordinates of the classical particles are carefully chosen.

Owing to the complex nature of the collision system, various reaction channels may occur in collisions between H_2^+ projectiles and H(1*s*) targets. They are listed as follows, where underlining denotes a fast particle:

$\underline{H}_2^+ + H(1s) \rightarrow \underline{H}_2^{+*} + H*$	elastic scattering or excitation (projectile or/and target),
$\underline{H}_2^+ + H(1s) \rightarrow \underline{H}^+ + \underline{H}^+ + H* + e$	projectile ionization and target excitation,
$\underline{H}_2^+ + H(1s) \rightarrow \underline{H}^+ + \underline{H}* + H*$	pure breakup of the projectile,
$\underline{H}_2^+ + H(1s) \rightarrow \underline{H}_2^* + H^+$	pure capture,
$\underline{H}_2^+ + H(1s) \rightarrow \underline{H}* + \underline{H}* + H^+$	dissociative capture,
$\underline{H}_2^+ + H(1s) \rightarrow \underline{H}^+ + \underline{H}^+ + H^+ + 2e$	projectile and target ionization,
$\underline{H}_2^+ + H(1s) \rightarrow \underline{H}_2^{+*} + H^+ + e$	target ionization and projectile excitation,
$\underline{H}_2^+ + H(1s) \rightarrow \underline{H}* + \underline{H}^+ + H^+ + e$	target ionization and projectile fragmentation.

Therefore, particular attention is devoted to define tests for ending the integration of the Hamilton equations along with an unambiguous identification of the reaction channels.

II. THEORY

A. Dynamics

We consider the five-body classical collision system (see Fig. 1) composed by the molecular projectile (two protons P_1, P_2 and one electron) and the atomic H target (one proton P_3 and one electron). The center of mass of the H target is put at the origin of a fixed referential *Oxyz*. The center of mass of the two protons P_1, P_2 initially lying in the plane *Oxz* is put at a large distance R_{in} from O, and at a distance b from the *Oz* axis defining the impact parameter. The initial velocity vector **V** of the projectile is along the *Oz* direction. In Fig. 1, θ defines the orientation of the H_2^+ molecular axis with respect to the *Oz*. The H_2^+ molecular axis is first pseudorandomly orientated by sampling θ between 0 and $\pi/2$. The OP_1P_2 plane is then pseudorandomly orientated with respect to the *Oxz* plane through a rotation of angle φ around the *Oz* axis sampled between 0 and 2π; correlatively this rotation is applied to all the coordinates of the three particles of the projectile. We outline in Sec. II B the classical method for the simulation of a stable dynamical molecule H_2^+ which, in another connection, is described in detail elsewhere [9].

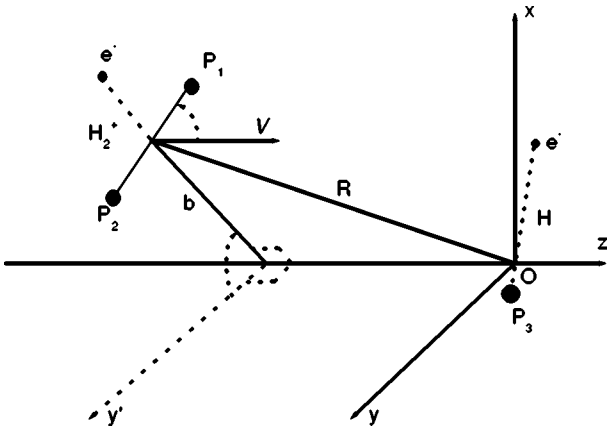

FIG. 1. Geometrical arrangement for a $H_2^+ + H(1s)$ collision (see text). The origin of the fixed coordinate frame is at the center of mass of the hydrogen atom (P_3, e^-).

The initial conditions for the H(1*s*) target are sampled as usual from a microcanonical distribution in space and momentum variables [1], following the method of Reinhold and Falcón [11].

The Hamiltonian of the system contains the kinetic energy of all the particles and their mutual Coulomb interactions,

$$H = \sum_i \frac{p_i^2}{2m_i} + \sum_i \sum_{j \neq i} \frac{z_i z_j}{r_{ij}},$$

where p_i, m_i, and z_i are, respectively, the momentum, the mass, and the charge of the particle i, and r_{ij} is the distance between the particles i and j.

For a given set of initial conditions, the 30 classical Hamilton equations of the collision system are solved numerically using a fourth-order Runge-Kutta integration method with a variable time step since a very close approach of two particles requires a very small integration step [1]. The integration is ended when the exit tests, described elsewhere, to identify the various reaction channels are fulfilled.

TABLE I. Coordinates (in a.u.) for the initial positions and momenta of the three classical particles used in the simulation of the H_2^+ molecular ion in its first vibration ground state. The electron momentum is just given as guidance (see text).

Particles	x	y	z	v_x	v_y	v_z
e^-	0.475	0.0	0.550	0.0	1.0566	0.0
p_1	0.0	0.0	1.415	0.0	0.0	0.0
p_2	0.0	0.0	−1.415	0.0	0.0	0.0

For a number of trajectories used in the large enough calculations, the classical cross section for a particular reaction P is defined as usual by

$$\sigma_P = \frac{N_P}{N_{tot}} \pi (b_{\max}^2 - b_{\min}^2),$$

where N_{tot} is the total number of trajectories used in the calculations, N_P is the total number of trajectories leading to the reaction P, and $b_{\min}$ and $b_{\max}$ are set for the limits of the impact parameter range.

This classical cross section is generally associated with a standard deviation given by

$$\Delta\sigma_P = \sigma_P \left(\frac{1}{N_{tot}} - \frac{1}{N_P} \right)^{1/2}.$$

We have also determined the final n distributions of the hydrogen fragments produced in the electron capture and fragmentation processes by using the method of Becker and MacKellar [12]. Finally, the probabilities $P(b)$ for the various reactions versus the impact parameter have also been calculated.

B. The dynamical H_2^+ molecule

As described in the Introduction, the vibration motion of the two protons H_2^+ correlated with the motion of the electron is simulated by solving the Hamilton equations for the three classical particles interacting through pure Coulomb interactions. We recall that this method conserves the electronic energy of the molecule (fixed initially to the experimental value of the electronic ground state in its first vibration level) during the integration of the Hamilton equations.

As done by Greenspan [9], we put initially the two protons at rest symmetrically at distances z, $-z$ in the reference frame *Oxyz*, and the electron is put in the plane *Oxz* with a velocity vector perpendicular to this plane. It is important to determine exactly the velocity of the electron from the value of the H_2^+ energy and from the positions of the two protons and that of the electron. Then the Hamilton equations are integrated and the set of the parameters fixing the positions of the three particles is changed until a large number of vibrations of the molecule is obtained. Finally, the parameters are more accurately adjusted in order to approach the best experimental vibration frequency and equilibrium distance of H_2^+ [13]. The best agreement with the experimental data is obtained for the initial position coordinates of the three particles which are reported in Table I, the energy of the first vibration (v=0) ground-state level of the molecule being set to −0.596 467 a.u. As pointed out before, when using these parameters to reproduce the vibration of the molecule, it is important to determine precisely the velocity component of the electron. Therefore, the value of the electron velocity is just reported in Table I for our guidance. It is important to note also that all the calculations have to be performed using a code compiled in 64-bit words. Thus, an average over 12 oscillations gives calculated values of 1.109 Å for the bond length and of 1.502×10^{-14} s for the vibrational period, which compare well to the experimental values of 1.070 Å and 1.450×10^{-14} s, respectively. We have verified that the stability of this classical and dynamical molecule is not changed after several hundreds of oscillations. Then the position and momentum coordinates for the electron and those for the protons are stored for a few oscillations of the molecule. These data are used afterwards in the collision problem to determine the initial conditions of the H_2^+ projectile by Monte Carlo sampling. It has to be noted that for any point of this sampling, the position and momentum coordinates refer to the fixed reference frame *Oxyz*, with the two protons on the *Oz* axis and the center of mass of the two protons put in O. For the collision problem (see Fig. 1), it is the center of mass of the H atom which is put in O, the H_2^+ molecule being set and oriented as described in the previous section.

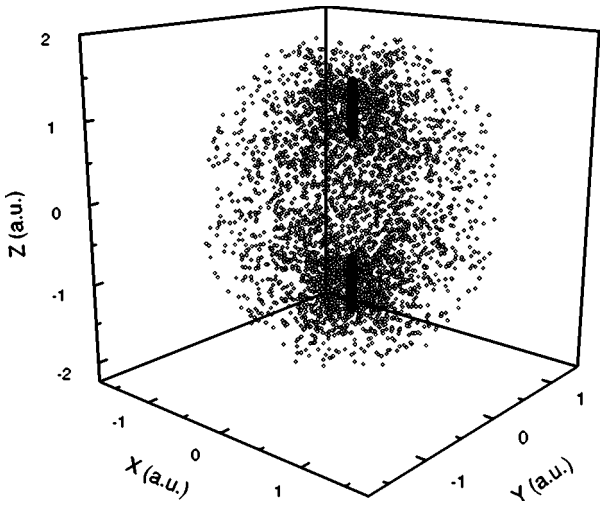

FIG. 2. Three-dimensional representation of the electronic cloud of the classical H_2^+ molecular ion along with the vibration motion of the protons.

We show in Fig. 2 the electronic cloud along with the motion of the two protons obtained from our classical calculations, indicating the relevance of the present model to represent the usual electronic density for an H_2^+ molecule.

C. Exit tests of the Hamilton equation integration

In order to proceed to the identification of the various reaction products, the Hamilton equations for each trajectory have to be first integrated from R_{in} up to a large distance R_{out} (500 a.u.) between the center of mass of the molecule and that of the hydrogen target. By varying R_{in} from

10 a.u. to 35 a.u., we have found that the value of 25 a.u. is appropriate for starting the integration of the Hamilton equations; from this distance, the interaction between the molecular ion H_2^+ and the neutral hydrogen atom becomes quite negligible. Then the total electronic energies $E_{e_i}^{H_2^+}$ and E^{H_2} of the molecules H_2^+ and H_2, respectively, and the binding energies $E_{e_i p_j}^{H}$ of each electron $e_i (i=1,2)$ with respect to each proton P_j ($J=1,2$ for the projectile and $J=3$ for the target) are calculated. We have not excluded the possibility that during the collision each electron can be associated with either the molecular ion or the hydrogen target. This allows us to identify the various reaction channels.

For example, since a stable molecule H_2 in its ground state dissociates for an electronic energy larger than $E_{diss}^{H_2} = -1 + 1/R_{P_1P_2}$, the formation of H_2 will occur if only the inequalities $E^{H_2} < E_{diss}^{H_2}$ and $E_{e_i p_3}^{H} > 0$ $(i=1,2)$ are both fulfilled, leading to the identification of the pure capture process.

In a similar manner, since the H_2^+ molecule in its ground state dissociates for $E_{diss}^{H_2^+} = -0.5 + 1/R_{P_1P_2}$, the pure breakup process of the projectile will occur if only the conditions $E^{H_2} > E_{diss}^{H_2}$, $E_{e_i}^{H_2^+} > E_{diss}^{H_2^+}$, $E_{e_{j\neq i} p_3}^{H} < 0$, $E_{e_i p_1}^{H} < 0$, and $E_{e_i p_2}^{H} > 0$ (or $E_{e_i p_2}^{H} < 0$ and $E_{e_i p_1}^{H} > 0$) are all fulfilled (or the other set of conditions obtained by interchanging the indexes i and j).

Finally, when the electronic energy of the H_2^+ molecule becomes larger than the Coulomb repulsion $1/R_{P_1P_2}$ between the protons, the ionization process of the H_2^+ molecule will be identified and tests have to be done also to know whether the H target is excited or ionized. All the exit tests to identify all the other reactions are easily obtained in a similar manner. If any of the exit tests is fulfilled, or if simultaneously more than one exit test is fulfilled (obviously, one and only one reaction is associated with each trajectory), the integration of the Hamilton equations for this trajectory has to be continued until the new value of R_{out}, set to twice the previous one, is reached. In order to obtain a very small percentage of nonidentified cases with respect to the large number of trajectories used in the CTMC calculations, this procedure is repeated up to five times if necessary.

III. RESULTS AND DISCUSSION

In order to compare the CTMC results with the experimental data of McGrath *et al.* [10], the calculations were mainly performed for impact energies between 20 keV and 100 keV. The calculations were extended to energies down to 2.5 keV, anticipating more experimental investigations in this low-energy range. Moreover, recent CTMC calculations have been shown to be quite reliable for predicting single-electron capture into *nl* final subshells as well as polarization of emission lines from these subshells in collisions between multicharged ions with neutral alkali-metal atoms at low energies [14]. Therefore, it would be interesting to check the validity of the CTMC method at low energies in the case of $H_2^+ - H(1s)$ collisions. The CTMC calculations were also extended up to 1000 keV since the CTMC method is usually expected be quite accurate at high energies. In this high-energy range, some experimental results are available [15] but do not allow us, however, detailed comparisons as with the data of McGrath *et al.* [10]. Therefore, we have mainly focused our attention on the discussion of the CTMC results for the 20–100 keV energy range.

A large number of trajectories (between 15 000 and 500 000 according to the energy) were used in the calculations in order to obtain small statistical errors. We found that the maximum value b_{max} of the impact parameter which contributes to the total cross-section values of the main reactions varies between 5.6 a.u. at the lowest energies and decreases down to 4.4 a.u. at 100 keV and to 3.5 a.u. at 1000 keV.

The calculated CTMC total cross sections, for each process under investigation, are reported in Table II and compared with the experimental data of McGrath *et al.* [10] in Figs. 3–8. In spite of some discrepancies for some individual reactions, our CTMC results show an overall agreement with the experimental data either for the order of magnitude of the cross sections or their variations with the impact energy. In particular, the relative importance of the various cross sections is well reproduced. As observed experimentally, the pure capture and the pure breakup of the molecule are found to be the dominant processes at low energies and decrease continuously with increasing energies, when the ionization of the target and the pure capture dominate at 100 keV. At higher energies, the CTMC calculations show that the ionization of the target remains the dominant process, goes through a maximum at about 125 keV, and then decreases. Above 150 keV, the pure breakup of the projectile becomes the dominant process after the process of ionization of the target, as well as the processes involving the ionization of the projectile. Let us consider now each of the various reaction paths.

Figure 3 shows the cross sections for the reaction path involving the projectile ionization (leading to Coulomb explosion) with the target being excited or not,

$$\underline{H}_2^+ + H(1s) \rightarrow \underline{H}^+ + \underline{H}^+ + H^* + e.$$

It can be seen that the CTMC cross sections are within the experimental error bars except below 50 keV, where the CTMC cross sections are higher. As expected, the ionization cross sections decrease when the impact energy decreases. But presently, the CTMC cross sections decrease much too slowly compared to the experimental ones and exhibit oscillations up to energies of 400 keV. More experimental measurements for this reaction are desirable in the low- and high-energy ranges to test further the CTMC results. For this reaction path, the CTMC calculated *n*-distribution indicates that the H target remains in its ground state.

Figure 4 presents the cross sections for the reaction path involving the projectile ionization (leading to Coulomb explosion) with target ionization,

$$\underline{H}_2^+ + H(1s) \rightarrow \underline{H}^+ + \underline{H}^+ + H^+ + 2e.$$

Here, the agreement is good at low energies, but above 80 keV the experimental data deviate from the CTMC results and indicate saturation when the CTMC cross sections continue to increase up to a maximum at 300 keV. Such a saturation for ionization processes, which occurs at relatively

TABLE II. CTMC calculated cross sections for the various reaction channels (as indicated in the table) which may occur in collisions between H_2^+ and H(1*s*) versus the collision energy.

	Cross sections ($\times 10^{-16}$ cm^2)						
Energy (keV)	Projectile ionization and target excitation	Pure breakup of the projectile	Pure capture	Dissociative capture	Target ionization and projectile excitation	Target ionization and projectile fragmentation	Projectile and target ionization
2.5	0.302±0.024	2.250±0.062	3.131±0.071	0.217±0.020	0.228±0.020	0.064±0.011	0.0018±0.0018
5	0.246±0.020	2.022±0.057	3.189±0.067	0.243±0.019	0.235±0.019	0.038±0.008	0
10	0.239±0.018	1.732±0.047	3.158±0.062	0.232±0.018	0.402±0.023	0.095±0.011	0.0014±0.0014
15	0.216±0.018	1.691±0.048	3.193±0.064	0.211±0.017	0.455±0.025	0.112±0.013	0
20	0.259±0.017	1.456±0.040	3.290±0.057	0.235±0.017	0.525±0.024	0.144±0.013	0.0011±0.0011
30	0.251±0.017	1.275±0.037	3.151±0.056	0.253±0.017	0.792±0.030	0.187±0.015	0.0046±0.0023
40	0.290±0.016	1.141±0.031	2.867±0.047	0.250±0.015	0.959±0.029	0.267±0.015	0.012±0.003
50	0.283±0.015	0.875±0.026	2.690±0.043	0.239±0.014	1.162±0.029	0.315±0.016	0.024±0.004
60	0.281±0.013	0.840±0.023	2.323±0.037	0.222±0.012	1.286±0.028	0.344±0.015	0.032±0.005
70	0.349±0.014	0.749±0.020	1.907±0.032	0.210±0.011	1.417±0.028	0.393±0.015	0.048±0.005
80	0.364±0.013	0.662±0.018	1.630±0.027	0.196±0.010	1.559±0.026	0.406±0.014	0.074±0.006
90	0.310±0.011	0.589±0.015	1.451±0.024	0.163±0.008	1.678±0.025	0.427±0.013	0.076±0.006
100	0.284±0.010	0.545±0.013	1.200±0.020	0.160±0.007	1.734±0.023	0.423±0.012	0.092±0.006
125	0.327±0.006	0.504±0.007	0.737±0.009	0.1005±0.0033	1.775±0.013	0.443±0.007	0.138±0.004
150	0.313±0.010	0.482±0.013	0.493±0.013	0.0693±0.0049	1.752±0.023	0.432±0.012	0.173±0.008
200	0.264±0.009	0.444±0.012	0.224±0.009	0.0293±0.0032	1.628±0.022	0.359±0.011	0.197±0.009
300	0.184±0.006	0.340±0.008	0.069±0.004	0.0060±0.0011	1.351±0.016	0.271±0.007	0.212±0.007
400	0.208±0.006	0.331±0.007	0.0269±0.0021	0.00164±0.00052	1.084±0.013	0.175±0.005	0.186±0.006
500	0.195±0.005	0.298±0.006	0.0110±0.0012	0.00070±0.00031	0.963±0.011	0.129±0.004	0.155±0.005
750	0.166±0.003	0.260±0.004	0.0035±0.0005	0.00015±0.00010	0.755±0.007	0.091±0.003	0.127±0.003
1000	0.137±0.003	0.202±0.003	0.0014±0.0003	0.00005±0.00005	0.626±0.006	0.067±0.002	0.104±0.002

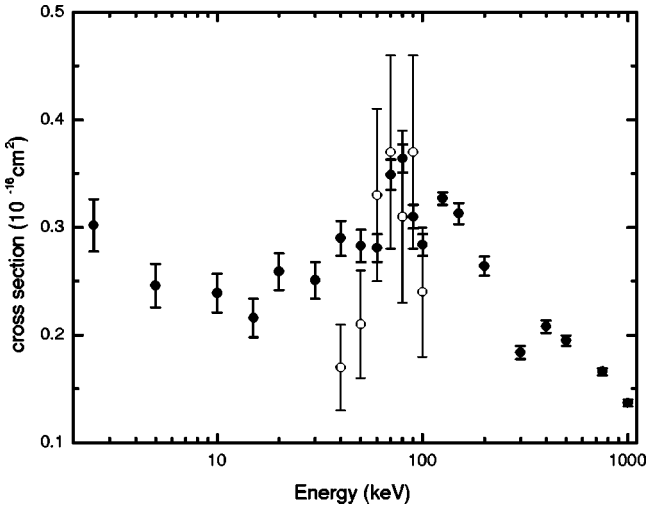

FIG. 3. Cross sections for projectile ionization with the target being excited or not. Open circles: McGrath data [10]. Full circles: present CTMC results.

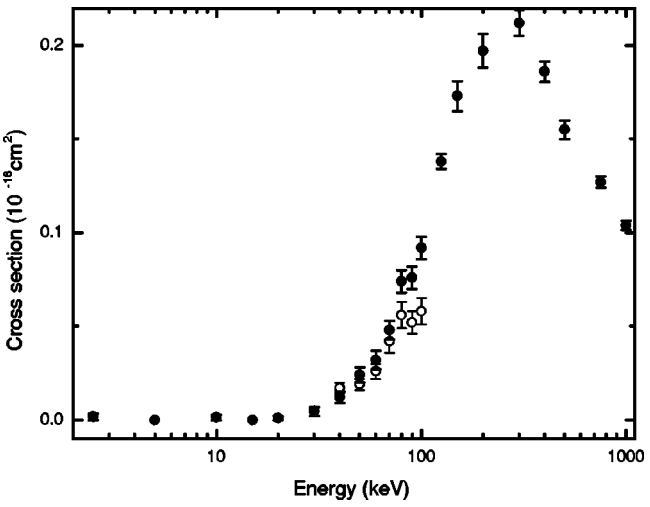

FIG. 4. Cross sections for target and projectile ionization. Open circles: McGrath data [10]. Full circles: present CTMC results.

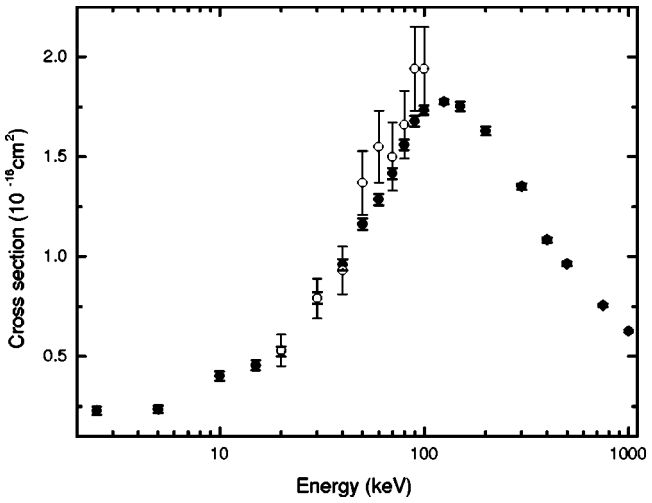

FIG. 5. Cross sections for target ionization with the H_2^+ ion being excited or not. Open circles: McGrath data [10]. Full circles: present CTMC results.

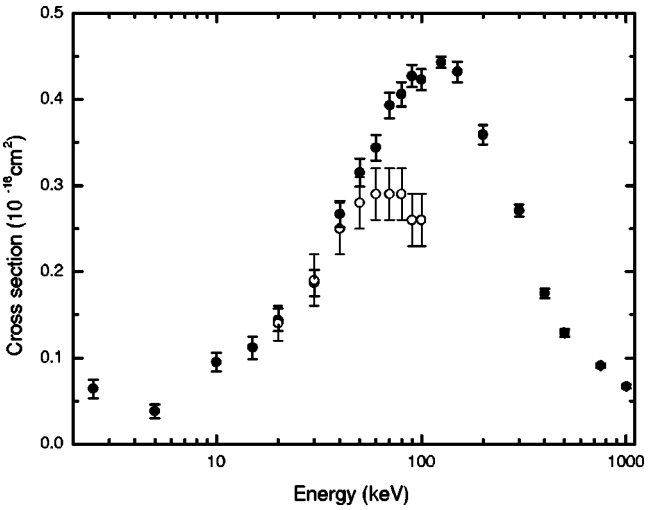

FIG. 6. Cross sections for target ionization and projectile fragmentation. Open circles: McGrath data [10]. Full circles: present CTMC results.

low energies in the experiment, is difficult to understand.

Figure 5 shows the cross sections for the reaction path involving the target ionization with the projectile being excited or not,

$$\underline{H}_2^+ + H(1s) \rightarrow \underline{H}_2^{+*} + H^+ + e.$$

The CTMC results are in good agreement with the experimental data over all the energy range. As expected, both measurements and CTMC calculations agree to find an increase of the cross sections with increasing energy, but more measurements are needed to verify the maximum in the CTMC cross sections at 125 keV.

Figure 6 shows the cross sections for the reaction path leading to the target ionization with fragmentation of the projectile

$$\underline{H}_2^+ + H(1s) \rightarrow \underline{H}^* + \underline{H}^+ + H^+ + e.$$

For low impact energies and up to about 50–60 keV, the CTMC results are in good agreement with the experimental data, but at higher energies the experimental data indicate a broad maximum which appears at about 125 keV in the CTMC calculations. As the experimental data for target ionization, without fragmentation or ionization of the projectile, are well reproduced by our CTMC results (see Fig. 5), the discrepancy observed at high energies is possibly due to an overestimation of the projectile fragmentation in the CTMC calculations. However, this would have been more understandable at low energies since then the collision proceeds over a larger time and possibly the $\underline{H}_2^+$ molecule might dissociate before undergoing a collision with the H target. However, we have discarded this possibility since no dissociation of the molecular ion is observed after integration of the Hamilton equations with the $\underline{H}_2^+$ projectile and H target being uncoupled.

For this reaction path, the CTMC calculations indicate that the fast $\underline{H}^*$ fragments are mainly in the ground state (about 97%) at the lowest energy, with also a small population of the $n=2$ state which increases up to about 30% at 100 keV when the population of the ground state decreases down to about 60%. The $n=1,2$ states have the same population (38%) at an energy of about 600 keV. At 1000 keV, the population of the $n=2$ state increases up to 40% and the population of the $n=1$ state decreases to 30%, indicating that the excitation of higher states of H becomes significant.

We present in Fig. 7 the cross sections for the reaction path leading to a pure breakup of the projectile with the H target being excited or not,

$$\underline{H}_2^+ + H(1s) \rightarrow \underline{H}^+ + \underline{H}^* + H^*.$$

The agreement is found to be very good above 50 keV but the CTMC results are slightly underestimated at low energy. Possibly, the change of the detector in the experimental work for the two lowest energies contributes to increase a little bit more the experimental uncertainties. Another source of uncertainty could also arise from the fact that the molecular ion used in the experimental work can be highly vibrationally excited and therefore favors the dissociative channels at low energy [16].

Our calculations indicate that for this reaction path, the pairs of states (n_1,n_2) for $\underline{H}^*(n_1)$ and $H(n_2)$ produced are mainly (1,1) for about 63% at the lowest energy, decreasing to about 46% at 100 keV and 28% at 1000 keV; then the pair (2,1) contributes to the pure breakup for about a constant percentage of 23% up to 100 keV and then increases to about 40% at 1000 keV. At the highest energies, the pairs of states (1,2), (2,1), and (3,1) contribute also to the reaction for a few percents. In particular, we have found that the contribution of the (1,2) pair reaches only 8% at 125 keV and decreases to 3% at 1000 keV, contrary to the assertion of McCartney *et al.* [16], based on the Bethe-Born calculations of Peek [17], that mainly the H target excited in the $n_2=2$ state contributes to the pure breakup for energies above about 40 keV. Our calculations demonstrate that, in all the energy range, the excited states of the H target play a minor role in the pure breakup of the $\underline{H}_2^+$ projectile, when the excited states of fast

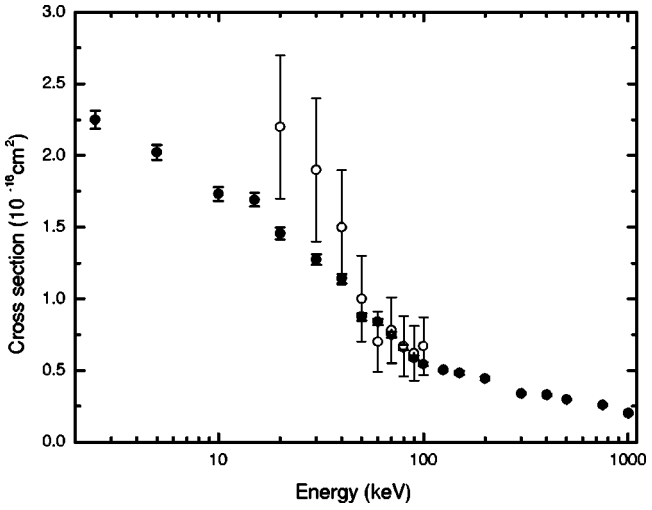

FIG. 7. Cross sections for pure breakup of the projectile. Open circles: McGrath data [10]. Full circles: present CTMC results.

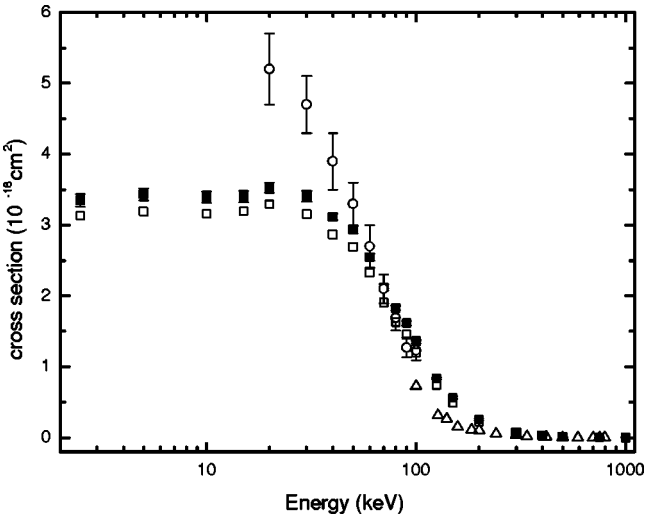

FIG. 8. Cross sections for the sum of the pure and dissociative captures (pc+dc). Open circles: McGrath data [10], open triangles: Sweetman data [15], and full squares: present CTMC results. The CTMC results for the pure capture (pc) alone are also reported in the figure (open squares) to show the small contribution of the dissociative capture. In this figure, the error bars for the CTMC values are of the order of the symbol size.

H* produced have a significant contribution. In another connection, it is interesting to notice that our calculations indicate that the H target remains in its ground state for more than 85%, in all the energy range, for the reaction path leading to elastic scattering or excitation (projectile or/and target).

Finally, for comparison with the experimental data, we present in Fig. 8 the sum of the cross sections for the pure capture and the dissociative capture,

$$H_2^+ + H(1s) \rightarrow H_2^* + H^+,$$

$$H_2^+ + H(1s) \rightarrow H^* + H^* + H^+.$$

Once again, the CTMC calculations reproduce quite well the measurements at high energies but underestimate the cross sections below 50 keV. This discrepancy between experiment and theory at low energies can be attributed to an underestimation of the pure capture process since, as it may be seen in the figure and Table II, the CTMC calculations indicate that the contribution of the dissociative capture is negligible in all the energy range, as suggested by McGrath *et al.* [10]. We have also reported in Fig. 8 the experimental data of Sweetman [15] obtained in the 100–780 keV energy range, which show an overestimation of the cross sections by the CTMC method at high energies. It is worthwhile to notice, however, that the experimental value of Sweetman [15] at 100 keV is smaller than the measurement of McGrath *et al.* [10] at 100 keV by a factor of about 1.75, indicating a possible normalization problem in the experiment; moreover, Sweetman has found that about 70% of the capture processes result in the dissociation of H_2, contrary to the CTMC calculations as discussed above. Finally, it is interesting to notice that our CTMC cross sections follow on the whole the unified cross-section scaling of Janev [18] for electron capture from excited hydrogen atoms by multicharged atomic ions. The CTMC cross sections for the capture processes take an almost constant value of about 3.4×10^{-16} cm^2 below 30 keV when the scaled cross sections go to a constant value of about 5×10^{-16} cm^2; at high energies, the CTMC cross sections are clearly overestimated. These discrepancies between the CTMC results and the unified cross-section scaling of Janev [18] may be due to the influence of the structure of the ionic projectile, in particular at low energies, since the impact parameters which contribute to the cross-section values are always less than about 4 a.u. At high energies, the influence of the molecular structure of the projectile is more difficult to appreciate since the collisions become sudden and the impact parameters contributing to the values of the cross sections are smaller.

In order to test further our calculations, we compare in Fig. 9 the CTMC calculated cross sections for total production of fast protons with those measured by McClure [19] and the ones extracted from the partial cross sections of McGrath *et al.* [10]. One can observe that all the sets of data are in good agreement in the 10–100 keV energy range. However, the CTMC cross sections increase continuously when the impact energy decreases, contrary to the experimental cross sections of McClure [19], which decrease quickly below 10 keV. At 2.5 keV, the discrepancy is about a factor of 2. This discrepancy is not yet clearly understood and needs more experimental investigations. We report also in Fig. 9 the measurements of Sweetman [15], which are seen to be smaller than the CTMC values, but also smaller than the experimental value of McGrath *et al.* [10] at 100 keV, indicating again a possible problem of normalization in the experiment, as noticed above for the capture processes.

Finally, we report in Fig. 10 the CTMC ratio of total production of two fast H^+ fragments over the total production of only one fast H^+ fragment. There are compared with those obtained experimentally by McCartney *et al.* [16] in the range 50–100 keV, and from the experimental data of

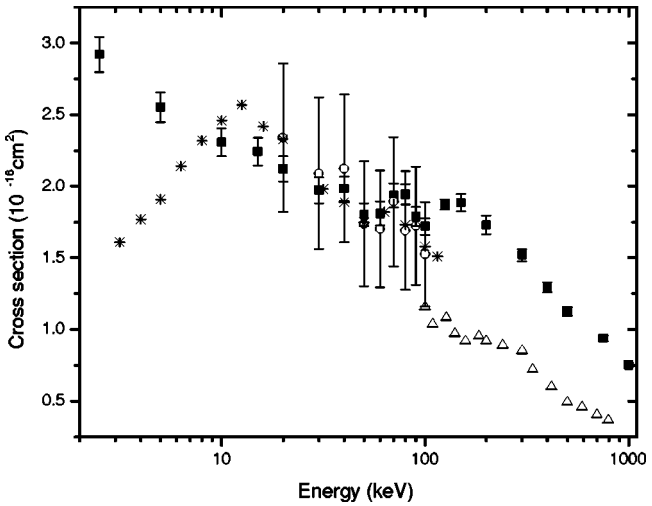

FIG. 9. Cross sections for total production of fast $\underline{H}^+$ ions. Open circles, McGrath data [10]; crosses, McClure data [19]; open triangles, Sweetman data [15]; and full squares, present CTMC results.

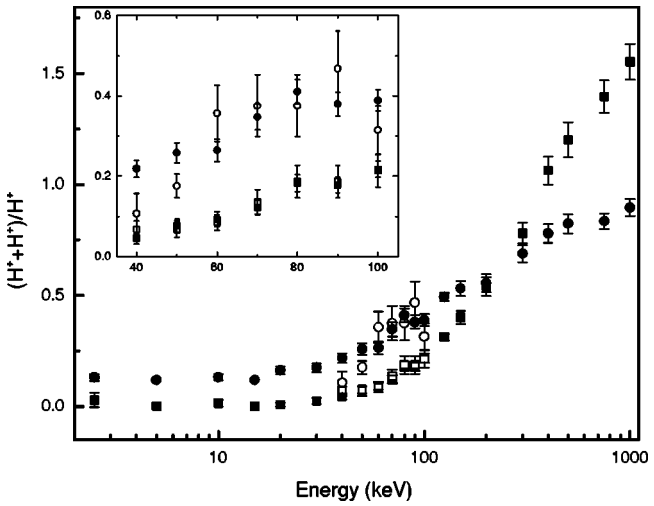

FIG. 10. Fast $(\underline{H}^+ + \underline{H}^+)/\underline{H}^+$ fragmentation ratio for H_2^+ projectile ions in collision with H(1*s*), see text. The full squares are the CTMC results which are compared with the measurements of McCartney *et al.* [16] (open squares) done in coincidence with the production of slow H^+. The full circles are the CTMC results which are compared with the noncoincidence measurements of McCartney *et al.* [16]. The figure has been enlarged in the 40–100 keV energy range to show more clearly the comparisons with the experimental data.

McGrath *et al.* [10] at 40 keV. The agreement is quite good. We compare also in the same figure the CTMC ratio of two fast $\underline{H}^+$ production over one fast $\underline{H}^+$ production in coincidence with the production of one slow H^+ (ionization of the target) with those obtained experimentally by McCartney *et al.* [16] and, at 40 keV, from the data of McGrath *et al.* [10] (it has to be noted that in the 50–100 keV energy range, the ratios obtained from the data of McGrath *et al.* [10], in coincidence or not, are quite compatible with those of McCartney *et al.* [16], but with larger error bars since they are determined from the individual cross sections). Now the agreement between CTMC calculations and the experimental data obtained in coincidence measurements is seen to be very good over all the energy range, in spite of the discrepancies observed at high energies between experiment and theory for the individual cross sections (see Figs. 4 and 6). Finally, Fig. 10 indicates clearly that, in all the energy range, the production of one fast proton is always larger than the production of two fast protons but tends to equilibrium at high energies.

IV. CONCLUSION

We have shown that a dynamical classical representation of the H_2^+ molecular ion is feasible without invoking any non-Coulomb model potential. When using pure Coulomb interactions between the particles, it is a careful determination of the initial positions and momenta of the particles, along with an accurate integration of the Hamilton equations, which prevents dissociation or autoionization of the molecule. This classical description of the molecule has been used in CTMC calculation for analyzing collisions between H_2^+ projectiles with H targets in the 2.5–1000 keV energy range. The cross sections for several reaction channels have been determined and compared with experimental data. The fair overall agreement observed between experimental data and CTMC results allows us to be confident in this classical simulation of a dynamical molecule. However, more experimental works at low energies, and also at high energies, are needed to test further the validity of the CTMC method. Extension of this work to the analysis of the energy and the angular direction of the fragments produced would be useful to get some insights into the physics of the various collision processes. It would be interesting also to simulate the H_2^+ molecular ion in the first excited vibration levels in order to see their role during the collision. We have also been able to describe a dynamical H_2 molecule in its first vibration ($v=0$) ground-state. Presently, work is in progress for studying collisions of multiply charged ion projectiles with H_2 targets in order to analyze the fragments produced in various reactions.

ACKNOWLEDGMENT

CTMC calculations were performed at CEA Saclay on Fujitsu VPP5000 and NEC SX6 computers under Contract No. P65.

[1] R. Abrines and I. C. Percival, Proc. Phys. Soc. London **88**, 861 (1966).
[2] L. Meng, C. O. Reinhold, and R. E. Olson, Phys. Rev. A **42**, 5286 (1990); **40**, 3637 (1989).
[3] C. Illescas and A. Riera, Phys. Rev. A **60**, 4546 (1999); J. Phys. B **31**, 2777 (1998).
[4] F. Sattin and L. Salasnich, Phys. Scr. **58**, 464 (1998).
[5] C. L. Kirschbaum and L. Wilets, Phys. Rev. A **21**, 834 (1980).
[6] J. S. Cohen, Phys. Rev. A **56**, 3583 (1997).
[7] C. J. Wood and R. E. Olson, Phys. Rev. A **59**, 1317 (1999).
[8] R. E. Olson and C. R. Feeler, J. Phys. B **34**, 1163 (2001).
[9] D. Greenspan, Phys. Scr. **55**, 277 (1997); **52**, 267 (1995).
[10] C. McGrath, M. B. Shah, P. C. E. McCartney, and J. W. McConkey, Phys. Rev. A **64**, 062712 (2001).
[11] C. O. Reinhold and C. A. Falcón, Phys. Rev. A **33**, 3859 (1986).
[12] R. L. Becker and A. D. MacKellar, J. Phys. B **17**, 3923 (1984).
[13] G. Herzberg, *Molecular Spectra and Molecular Structure. I. Spectra of Diatomic Molecule* (Van Nostrand Reinhold, New York, 1950).
[14] See, for example, C. Lauhlé, E. Jacquet, Ph. Boduch, M. Chantepie, N. Ghérardi, X. Husson, D. Lecler, and J. Pascale, J. Phys. B **30**, 2899 (1997); E. Jacquet, M. Chantepie, Ph. Boduch, C. Lauhlé, D. Lecler, and J. Pascale, *ibid.* **32**, 1151 (1999); E. Jacquet, H. Kucal, V. Bazin, Ph. Boduch, M. Chantepie, G. Cremer, C. Lauhlé, D. Lecler, and J. Pascale, Phys. Rev. A **62**, 022712 (2000).
[15] D. R. Sweetman, Proc. R. Soc. London, Ser. A **256**, 416 (1960).
[16] P. C. E. McCartney, C. McGrath, J. W. McConkey, M. B. Shah, and J. Geddes, J. Phys. B **32**, 5103 (1999).
[17] J. M. Peek, Phys. Rev. **140**, A11 (1965).
[18] R. K. Janev, Phys. Lett. A **160**, 67 (1991).
[19] G. W. McClure, Phys. Rev. **153**, 182 (1967).